The WildFire Experiment (WiFE): Observations with Airborne Remote Sensors

by L.F. Radke • T.L. Clark • J.L. Coen • C.A. Walther • R.N. Lockwood • P.J. Riggan • J.A. Brass • R.G. Higgins

RÉSUMÉ

Les capteurs aéroportés ont longtemps constitué la pierre angulaire de la recherche dans le domaine des feux de forêt et, depuis peu, les modèles tridimensionnels de comportement d'incendie couplés entièrement avec l'atmosphère commencent à montrer un niveau élevé de vraisemblance. Les expériences WiFE (WildFire Experiments) tentent de combiner les capteurs aéroportés et les observations multi-capteurs dans le développement et la validation des modèles d'incendie. Un ensemble de capteurs fournis par diverses agences a été installé sur l'appareil Lockheed C-130 de la National Science Foundation et du National Center for Atmospheric Research (NCAR) pour les besoins du projet. Plusieurs de nos objectifs ont été atteints au cours d'une seule saison d'observations dans le contexte de ce programme préliminaire de validation du concept. En 1998, nous avons tenté d'observer les feux les plus importants qu'il était possible de trouver à l'intérieur d'un rayon d'environ 1500 km de notre basé au Colorado (~3 heures de temps de vol). Dans la planification de notre mission, avec l'aide du National Fire Information System, nous avons recherché les incendies ayant des comportements extrêmes et complexes et nous avons pu localiser de vastes feux de forêt de forte intensité qui ont été remarquablement bien imagés par l'ensemble des capteurs.

SUMMARY

Airborne remote sensors have long been a cornerstone of wildland fire research, and recently three-dimensional fire behaviour models fully coupled to the atmosphere have begun to show a convincing level of verisimilitude. The WildFire Experiment (WiFE) attempted the marriage of airborne remote sensors, multi-sensor observations together with fire model development and verification. An interagency array of sensors was mounted on the research Lockheed C-130 aircraft of the National Science Foundation and the National Center for Atmospheric Research (NCAR) for this project. Many of our observational goals were reached in a single fire season in this preliminary proof of concept program. In 1998, we observed several large fires within about 1500 km of our base in Colorado (~3 hours flying time). In mission planning, assisted by the National Fire Information System, we sought extreme and complex fire behaviour and were able to locate some large high intensity wildfires that were superbly imaged by the sensor payload.

Keywords

The principle WiFE observing tools were:

- *Inframetrics Thermacam PM380 (TCAM) - A cooled 3-5 μm infrared (IR) high-speed imager (60Hz) that can clearly penetrate large amounts of smoke that are entirely opaque at visible wavelengths to reveal detailed fire dynamics.*
- *Extended-Dynamic-Range Imaging Spectrometer (EDRIS) - A NASA/United States Department of Agriculture (USDA) Forest Service-built cooled multi-channel (4) IR cross track line scanning imager which, while it produces only one image per overpass, has 500 nm (visible) to 10 μm (IR) images that clearly show where fires are located relative to geographic features.*
- *Airborne Imaging Microwave Radiometer (AIMR) - A 37 and 90 GHz passive microwave cross-track line scanner/imager with both vertical and horizontal polarizations in each wavelength channel. With this imager even the small fire-capping water clouds (pyrocumulus) do not obscure either the fire or the vegetation/fuels beneath.*

Successful field-verification of fire behaviour by coupled atmosphere fire models potentially could transform wildfire management.

Received: 27 August 1999/Revised: 20 June 2000

• Lawrence F. Radke, Terry L. Clark, Janice L. Coen, and Craig A. Walther are with the National Center for Atmospheric Research Boulder, Colorado, USA.

• Robert N. Lockwood and Phillip J. Riggan are with the United States Department of Agriculture Forest Service, Riverside, California, USA.

• James A. Brass and Robert G. Higgins are with the NASA AMES Research Center, California, USA.

INTRODUCTION

Wildland fire is a natural hazard of growing significance in North America. Each year wildfires scorch several million hectares with damage and control costs exceeding ten billion dollars per annum. As we now recognize that wildland fire is a necessary part of many natural ecosystems, fire researchers are being challenged to manage, control, and predict wildfire in entirely new ways. Simply rushing to extinguish every spark is no longer a sufficient strategy, even if it was practical. The sheer number of wildland fire starts in North America exceeds one hundred thousand each year, mostly started by lightening strikes. However in the usual course of events, only a few become truly large fires causing enormous amounts of damage and devastation. Further, many of these fires will self-extinguish and many, if left largely unattended, will produce significant ecological benefit. The real challenge for the managers of wildfires and the evolving landscape are predicting which wildfires will be large enough to warrant immediate and dramatic attention. A key part of meeting this challenge will be the development of fire behaviour models that incorporate the complexity of terrain, fuel distribution, density, and the evolving meteorological conditions. For such a model to be useful to forecast wildfire outcomes, models must be able to produce the full range of behaviour that results from interactions between a fire and its atmospheric environment. Properly nesting these physically complex extreme fire dynamics within coupled-atmosphere fire models of large fires is made more difficult by our inability to observe them at the needed temporal and spatial scales with the observing tools generally available to fire researchers. Naturally, the ability to model and predict the evolution of real wildfires allows us to confidently verify the model outputs, estimate costs and time needed for fire control, and begin to carry out model experiments that include various fire suppression strategies that can then be used to select the appropriate management plan.

The WiFE Project studied wild and prescribed fires in California, Montana, Idaho, and Colorado in the late summer of 1998. Several of these fires burned thousands of hectares as they ran uncontained, and two burned under the "Red Flag", the United States Department of Agriculture (USDA) Forest

Table 1.
WiFE Remote Sensing Instruments

Sensor Name	Builder & Customization	Resolution	FOV	Data Stream	Sensitivity	Temp. Range
Thermal Camera 380 (TCAM 380)	Inframetrics, Inc. Cryogenic sensor; Mechanically cooled	256 x 256 pixel platinum silicide focal plane array detector (~3m at 3km A.G.L.)	16°	12 bit digital & video data streams	< 0.1° C	– 10° C – 1500 °C
Extended Dynamic Range-Imaging Spectrometer (EDRIS)	NASA/US Forest Service; Nadir scanning Cross Track Radiometer Wavelengths 0.529-.680 (1.55-1.70μm , 3.95-4.05μm , 11.6-12μm)	2.6 m pixel at 3 km A.G.L.	±40° from nadir across the aircraft's track	16 bits capable only 12 bits recorded	< 0.1° C at 10 μm	– 27° C – 727° C
Airborne Imaging Microwave Radiometer (AIMR)	Built by MPB Technologies, Canada and adapted for WIFE by NCAR's Remote Sensing facility AIMR is coupled to the C-130 radar altimeter and inertial altitude reference. By changing antenna rotation rate it automatically creates a geometrically correct image regardless of airspeed, altitude, or modest departures from level in pitch & roll.	Receiver: 37 GHz & 90 GHz with vertical & horizontal polarization at both frequencies 3db beam width of 1° at 90 GHz yields a 50 m footprint at 3 km A.G.L.	±60° from nadir across the aircraft's track	4 Channels 12 Bits 0.5 Degrees spacing	< 1° C	– 20° C – 1500 °C

Service's most extreme condition of fire weather classification. The first Red Flag fire was observed near Summit, Montana and was part of a very large complex of lightning-ignited fires. The McDonald Creek fire in the Kootenai Complex (National Interagency Fire Center's nomenclature, http://www.nifc.gov/sitreport) received particular attention with its strongly ascending column of dark smoke capped by a vigorous pyrocumulus, an obvious signpost in an otherwise cloudless sky (4 September 1998). Though we were able to orbit over this fire and periodically sample through the smoke column, it remained completely cloaked in smoke and, despite heavy flames along the boundaries of the fire, flames were generally not visible to the eye. However, our remote sensing tools revealed some dramatic fire dynamics. The second Red Flag fire to be discussed, part of the Edna fire complex, burned uncontrolled in the scrub and grassland light fuels east of Riverside, California, and blackened nearly 32,000 hectares in just over 36 hours. Combining the three imaging remote sensors on a C-130 aircraft proved a real boon to the experimenters, even though the high speed IR imager (TCAM), the multispectral visible-IR line scanner (EDRIS), and the passive microwave imager (AIMR) did not offer precisely the same Field of View (FOV) simultaneously. The C-130's remote sensing payload is detailed in **Table 1**.

The C-130's flight characteristics also proved advantageous in ways we had not anticipated. The aircraft is sufficiently massive that vibrational problems were minimal and despite its ponderous appearance, it proved satisfactorily nimble in complex manoeuvres and its range and endurance proved ample for our program. We also describe herein some critical developmental work done from ground-based platforms in the paths of prescribed experimental fires in Canada and Australia.

Aircraft Motions and Fire Dynamics

A traditional task in airborne remote sensing is to register an image onto an earth reference system, which normally is made easier by holding the imager stationary aboard the platform in an inertial reference frame and by over-flying the target while very straight and level. Such a sampling strategy usually produces only one image per overhead pass. However, to observe the dynamic motions within a wildfire, a series of images must be registered onto a fixed earth reference. During WiFE, the TCAM IR imager was pointed downward with a pan and tilt mechanism while the C-130 executed a continuing pylon turn around the fire's central core several kilometres below. The pilot attempted to fix the centre of the turn, compensating for the mean wind by smoothly changing bank angle and power settings. Meanwhile, the TCAM operator simultaneously adjusted the pan and tilt to further centre the target, creating a complex combination of translational and rotational motions in the image sequence. The first analysis step was to remove these platform motions from the image sequence. This was straightforward, but numerically intensive.

Treating Apparent Motion

Both airborne and tower IR fire observations can require the extraction of platform motions before meaningful fire convective winds and other motions can be estimated. Pylon turns completely rotate the image about the pivot point about every two minutes, which imposes an apparent high amplitude counter-rotating vortex about the pivot point of the fire. Swaying towers, on the other hand, impose a translational and mostly sideways jitter to the image.

The method we chose to extract apparent motion is to minimize the function, Λ,

$$\Lambda=\sum[\phi(x,y,t)-\phi(x+\Delta x,y+\Delta y,t+\Delta t)]^2 \quad (1)$$

where $\phi(\vec{x},t)$ and $\phi(\vec{x},t+\Delta t)$ are two consecutive images 1/30 seconds apart. The resolution of the original images is reduced by averaging down a factor of five in the x- and y-directions to form ϕ. This data reduction has the effect of accentuating motion of the entire image and minimizes biases due to the local convection. In the case of the swaying tower, we found that the IR temperatures near the surface served this purpose. The Δx and Δy motions required to minimize Λ, are taken as the sum of translation and rotation such that

$$\Delta x=\Delta X-(y_{ij}-y_0)\sin(\delta\theta) \quad (2)$$

and

$$\Delta y=\Delta Y+(x_{ij}-x_0)\sin(\delta\theta) \quad (3)$$

where ΔX and ΔY are the two components of translation and $\delta\theta$ represents the incremental angle of rotation about the point (x_0, y_0) which is taken as the centre point of the image. The rotation components of Equations 2 and 3 are linearized to simplify the resulting matrix equations.

We minimize Λ with respect to ΔX, ΔY, and $\delta\theta$ obtaining a third order linear matrix. The system is solved iteratively by updating $\phi(x+\Delta x,y+\Delta y,t+\Delta t)$ until convergence is attained. We then progress to the next image. In this manner, we obtain a history of ΔX, ΔX, and $\delta\theta$ which we process to extract any obvious convective effects. For example, in the case of the swaying tower we expect integrated ΔX and ΔY to oscillate about zero. Since the data still contain significant noise at this stage, some detrending (or filtering) of the image registration data is necessary.

Figures 1a and **1b** show a history of the time-integrated values of ΔX and ΔY for 50 s of C-130 flight time over Glacier National Park. The units are in pixels and the results show a significant amount of platform translation resulting from the pan-tilt mechanism and aircraft motion. Applying these results to shift each frame to a common reference results in smoothly varying fields of convective motions with little detectable jitter due to all forms of platform motion. These estimates of platform motion were used to process the C-130 data in **Figure 2**. **Figure 2** provides corrected frames 920, 935, 950,

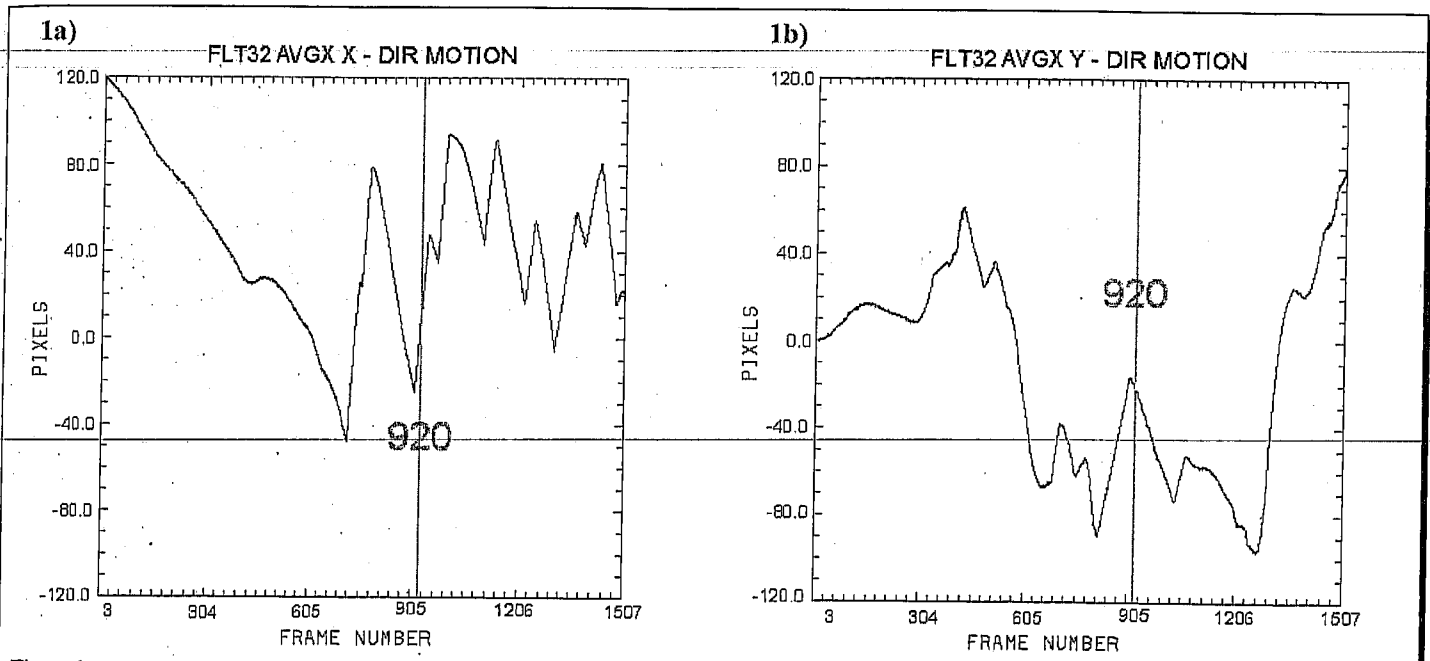

Figure 1.
A time history of the time integrated values of Δx and Δy for 50s (1500 image frames) of C-130 flight time over Glacier National Park. The x and y displacements for frame 920 (the first image in Figure 2) are marked on the graphs below.

and 965, which as **Figure 1** shows represents an interval of rapid x-y translational motion. The correction places these four images into a common georeference that is roughly equivalent to what would have been observed had the platform been fixed in space. This results in far more coherent views of the entire fire and surrounding spot fires during the period when extreme fire dynamics were observed (**Figure 7**), because changes in **Figure 2** are due only to time and not platform motion.

For most of the airborne IR data, we do not shift all frames to a common reference because we are flying around the fire, the perspective is changing with time and the process is extremely labour intensive. In this case, images are shifted to a common reference only for evaluation of fire winds that may involve between two and seven images.

Estimating Fire Winds from Image Analysis

The methods employed are a mixture of correlation techniques (as for the apparent motion analyses) and gradient methods that were developed using ideas from Horn and Schunck (1981), Nagel (1983), Verri *et al.* (1990), and Bab-Hadiashar and Suter (1995 and 1997). The methods used are usually called image flow analysis. In our analyses of prescribed crown fires in Canada's Northwest Territory (NWT), crowning wildfires in Montana, and grass fires in Australia's Northern Territory (NT), we used a gradient technique based on Bab-Hadiashar and Suter (1997) using robust statistics and least-squares minimization. For details on our method of extracting fire winds, see Clark *et al.* (1999). Probably the main difference between Clark *et al.* (1999) and the approach discussed here is that instead of minimization over the entire image, Clark *et al.* (1999) performed local minimizations on patches of data around each pixel, typically 7 by 7 pixels.

Figure 3 shows an example of winds analyzed from the NWT Plot 6 crown fire in 1997, where the TCAM was mounted on a tower ahead of the approaching fire. The figure shows two counter-rotating rising plumes/vortices on both sides of the figure, marked A and B. The more intense B vortex has many of the aspects of a corkscrew spiral. Note that since these features remain vertical with time, the systematic horizontal motions must be the result of vortex rotation. The wind vectors were derived using the image flow algorithm described in Clark *et al.* (1999), which estimated wind speeds of ± 30 m/s. This analysis was performed on 30 frame/s data that contained considerable noise due to JPEG compression, interlacing, recorder wow and flutter as well as (in other examples) regions of high electric charge on the camera's IR elements spilling onto their neighbours.

Figure 4 shows the fire updraft and horizontal wind velocity statistics derived over the 4.5 minute burn of Plot 6. The thin lines show the actual point extreme, whereas the thick lines follow the mean ± 5 standard deviations that represent the extreme values found in a large normally distributed data set. When values fall outside of this range, we assume that they are artifacts of our analysis procedure. The differences between these two estimates are believed to result from outliers that were otherwise missed by the data processor. Thus, the statistical estimates are the more meaningful results. Physically we interpret the decreasing updraft (W) extrema from about 0.5 to 3.5 minutes as following the history of the total sensible heat flux from the advancing fire front. The nearly constant and

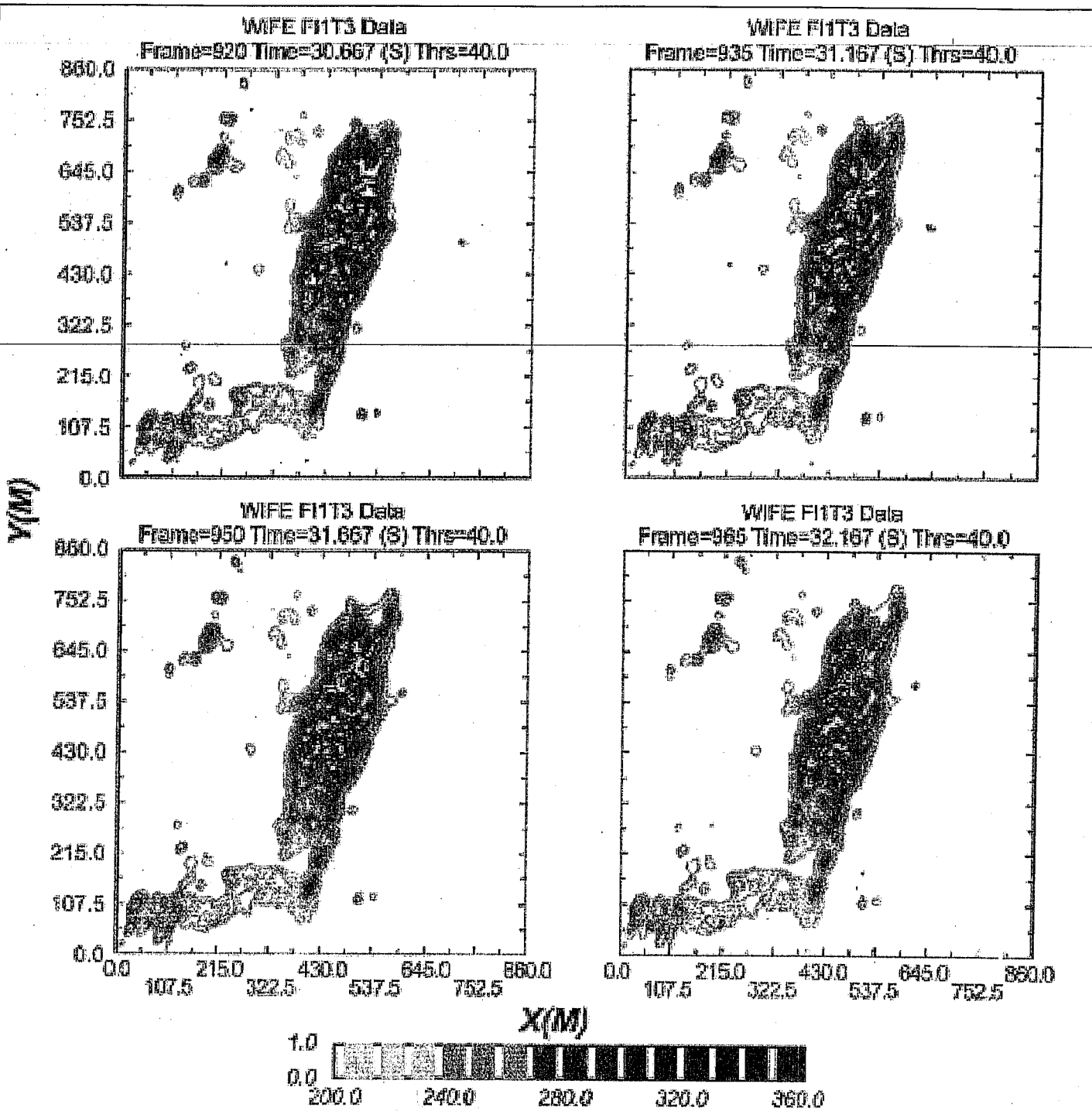

Figure 2.
The aircraft orbits the crown fire turning to the left at 3°s^{-1}. The camera-pointing angle is complicated by turbulence and the changes in bank angle needed to fly a pylon turn. Correcting digitally for the aircraft motion, these four images are georeferenced locked in place, allowing the perspective that would be attained if the aircraft and camera were stationary. The greyscale legend shows temperature in degrees Celcius.

small downdraft extrema reflects our observing position and a challenge of a nearly horizontal perspective. The downdrafts are effectively hidden at the rear of the fire. The U extrema differences (±) decrease physically for the same reasons that W (updraft) decreases with total sensible heat flux. The horizontal (U±) velocities represent the inflow air on the flanks of the fire.

Figure 5 shows an example of the wind patterns derived from a grass fire in the Australian NT near Darwin (Hughes

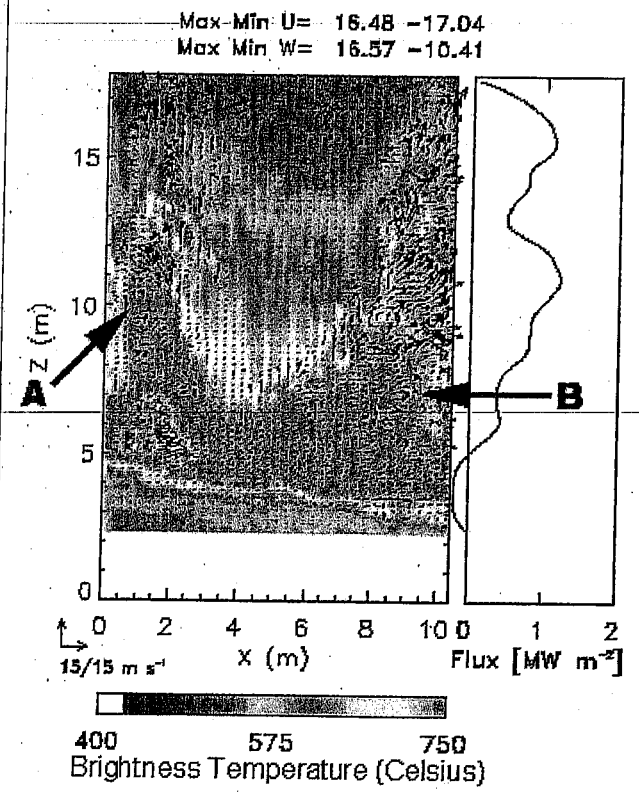

Figure 3.
Winds analyzed from the NWT Plot 6 crown fire in 1997. The fire is moving toward the observer. Note rotation in the intense feature on the right that has some aspects of a corkscrew spiral. The apparent vortex on the left, A, is counter-rotating with respect to the vortex on the right, B.

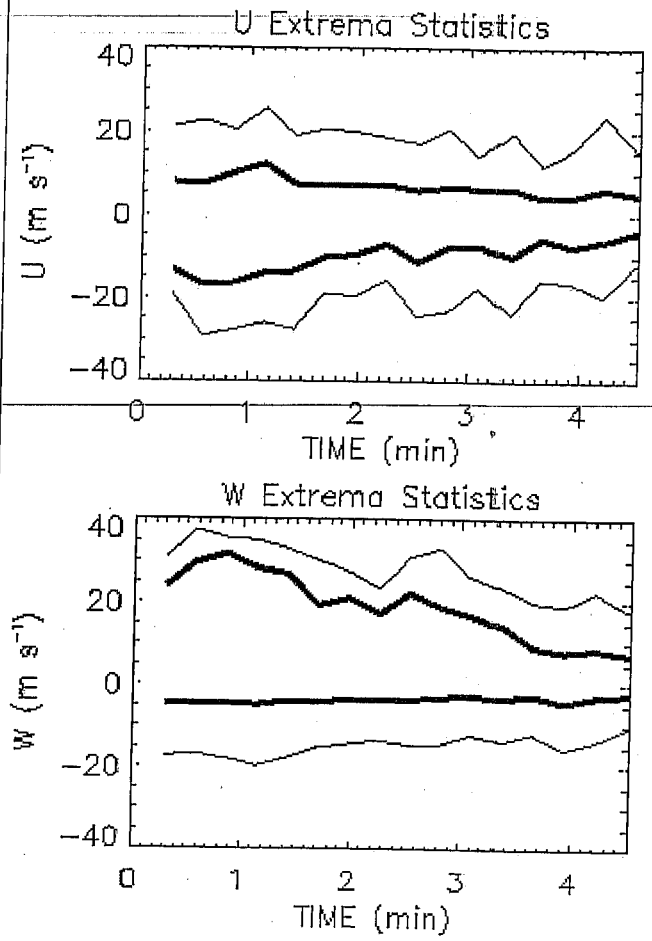

Figure 4.
Fire wind velocity statistics derived over the 4.5 minute burn of plot 6. The fire's sensible heat flux peaks at ~t=1 minute and then declines (not shown). This largely explains the trends in updraft (W) and horizontal winds (U). Thin lines are point extremes, while thick lines are ±5 standard deviations.

Airfield). The IR camera was mounted on a cherry picker about 200 m ahead of the fire; this figure shows just a small portion of the total image. The horizontal and vertical spatial scaling of the rising thermals is quite similar to that of the Plot 6 NWT crown fire, suggesting that fuel spacing is probably not the controlling factor in either case.

In **Figure 6**, taken from the C-130 during WiFE, we have removed the aircraft's rotational and translational motions and then focused on trackable hot features (probably flaming brands and embers). The view of the fire is plan from above so the flaming targets that are moving to the top of **Figure 6** are both rising into a convective column and moving rapidly in the horizontal x-y plane. Here, the fire has been advancing for some time toward the bottom of the page and vigorous combustion is largely isolated in the "L"-shaped region. The small features in the right half of the figure are believed to be small fuel "pockets" where combustion continues and not merely "hot spots". Air is rushing in largely on the fire's west flank, exiting at the upper right corner. The ascending flame is seen accelerating toward the top of the page and then spiralling to the right. Consistently organized motions exceeding 20 ms^{-1} can be found. Hints of vortex motion exist at the bend in the "L", suggestive of pillar-like fire whirls such as those shown in **Figure 3** that were observed near intense experimental fires.

Tilted Vortices, Fire Whirls, Hairpin Vortices and Other Dangerous Phenomena

As fires become larger and more convectively intense, even casual observers of fire dynamics are struck by the ubiquitous appearance of various rotational motions both within the fire structures and outside of them (Clark *et al.*, 1999). However, hairpin vortices, pillar-like vortices, violent forward bursting turbulent features, and numerous others in the NWT crown fire and WiFE data, that were easily identified using IR imagery (**Figure 2**) and temperature (T), would be difficult or impossible for observers to detect visually through smoke. The TCAM 60 Hz 3-5μm cooled imager, with its pixel footprint of approximately 6 m^2 from 3 km above ground level (A.G.L.), is well suited to identify such features (Radke *et al.*, 1991), even from the smoky skies above a fire.

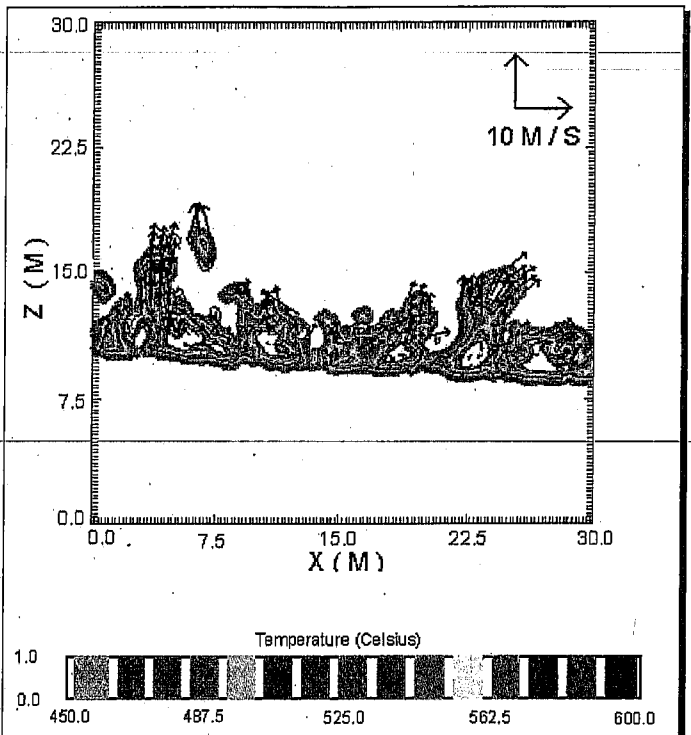

Figure 5.
Wind patterns derived from analysis of a grass fire in the NT near Darwin (Hughes Airport). Note the change in dimensional scale compared to Figure 3.

Fire whirls, a cousin of dust devils, are often found in the lee of intense fires where they are typically transient and usually travel somewhat to the right of the mean of the wind. Less frequently and less adequately explained are vortices that remain nearly stationary within a fire. In this case, convergence, due to fire-induced convection, leads to stretching and rotational intensification (Scorer, 1978). **Figure 7** (Frames 1 - 6) shows a remarkable series of images with imbedded vortices taken 0.75 seconds apart of a fire moving up a shallow canyon. Frame 1 begins the sequence and presents a fixed reference perspective plan view of the violent McDonald Creek wildfire. Seven horizontal rolls capped by apparent falling hot core vortices are marked in Frame 3. Note the even or wavelike spacing of the vortices on the right flank; approximately 30m separate these capping vortices from each other. Also marked on Frame 3 and 4 are linear horizontal roll-like structures forming in the interior of the conflagration. Such horizontal roll vortices have not been observed with remote sensors previously to our knowledge, but have been inferred indirectly as having occurred during crown fires (Pyne, 1996 and Haines, 1987). In those examples, "streets" of unburned, but scorched foliage were paralleled by rows of heavily burned canopy. Presumably the cool down draft side of the vortex kept the flames out of the crowns. Such explanations, at least partially, describe the conditions seen here. Frame 3 also shows some vortex intensification and lower roll twists within the fire when the roll feature increases in brightness temperature.

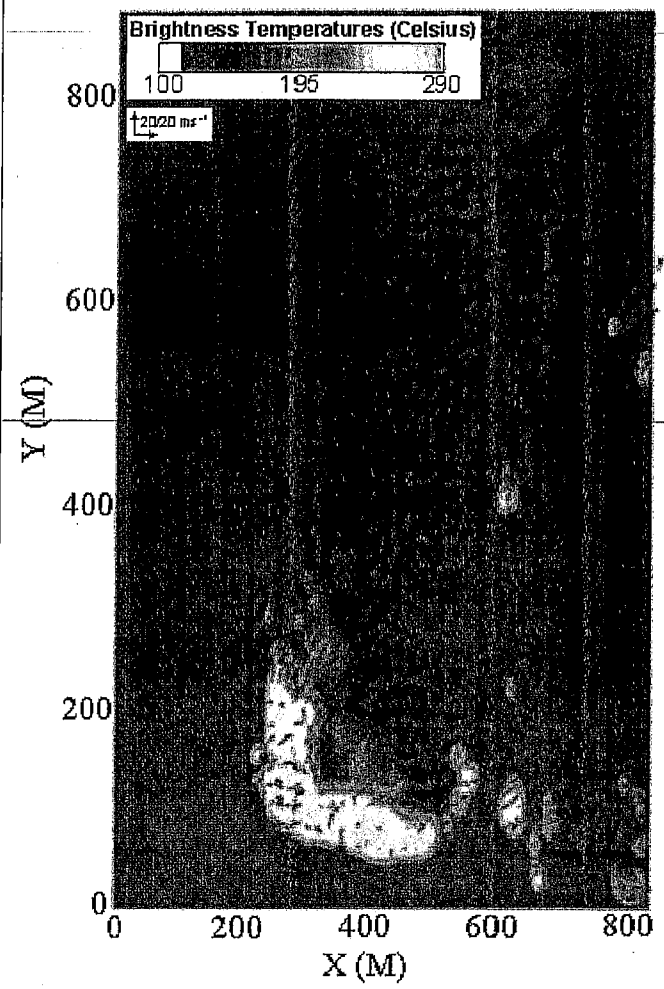

Figure 6.
Plan view of a ~10 hectare blaze on 23 September 1998 showing the air flow motions after the aircraft's translational and rotational motions are numerically removed. The temperature displayed is equivalent brightness, where emissivity equals one.

Next, focus on the vortex at the top right of the fire images in **Figure 7**, marked "FOD". A horizontal arm-like feature is seen beginning to develop in Frame 1, continues to develop in Frames 2 - 4, peaks in Frame 5 striking out horizontally nearly 150m at more than 100kph, and collapses in Frame 6 leaving hints of ignitions in its wake. The feature is dubbed the "Finger of Death" (FOD). The FOD is an unstable feature that is drawn back nearly as quickly as it advanced.

While the authors have seen other very hot fire vortices previously, here airborne remote sensing has documented an extremely hazardous phenomenon that is not only a remarkable mechanism for fire propagation and a threat to fire fighters, but one that is usually so cloaked in smoke that it would go unobserved. Indeed, while the C-130 wheeled above the centre of the wildfire, smoke obscured all traces of flame in the video data from a co-aligned colour video camera attached above the TCAM. It is not surprising that unusual atmospheric dynamic responses often appear with rapidly advancing fires in heavy fuels when we consider the heat

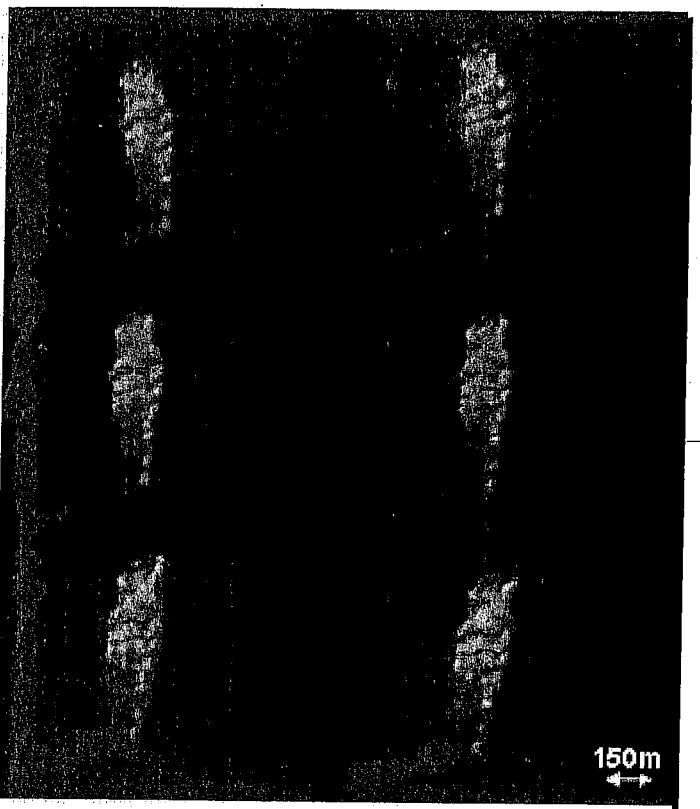

Figure 7.
Six plan view images in a time sequence, 0.75 seconds apart, of IR imagery from the McDonald Creek wildfire. Brightest colour (yellow) is the hottest. Seven horizontal rolls capped by apparent falling vortices are marked in Frame 3, the rolls and capping vortices are also apparent in the other frames. Two adjacent horizontal roll features are marked in Frames 3 and 4. The flame filled "Finger of Death" (FOD) vortex is marked with an arrow in each frame. The FOD is just beginning to develop in Frame 1, peaks horizontally in Frame 5, and collapses in Frame 6 leaving hints of fire spread in its wake.

release rates involved; for example, the dramatic, but moderately sized prescribed 150 x 150 m NWT crown fires exceeded 1 gigawatt for several minutes.

NCAR's Coupled Atmosphere – Fire Dynamics Model

An important component of these studies to understand the dynamics of wildfires is NCAR's coupled atmosphere-fire model, described in detail in Clark *et al.* (1996a, 1996b, and 1998). A three-dimensional, nonhydrostatic atmospheric prediction model has been coupled with a physically based wildfire model and is being used to study the complex interactions between fire and local winds.

The models are fully coupled in that evolving modelled atmospheric information is used to drive the propagation of the fireline, and the heat and moisture from the fire model is released into the modelled atmosphere, greatly changing atmospheric motions over a range of scales that encompasses the fine-scale, raging winds within the fireline to deep pyrocumuli that reach throughout the troposphere. The fire model itself uses a scheme in which four tracers identify the portion within each grid cell that is burning. These tracers can move with the wind at an empirical spread rate that depends on the local wind velocity and fuel characteristics, or they can back or move normal to the wind. As the modelled fire propagates, heat is released with time naturally, based on the type of fuel, so that fine fuels like grasses are consumed quickly, carrying the flaming front, while larger fuels if any are left behind to burn slowly. The heat and moisture from this combustion are distributed into the fluid dynamics model as heat and moisture fluxes near the surface.

This model is ideally suited for the WiFE studies, as it can simulate in detail the airflow over mountainous topography, like that of Glacier National Park. It can also incorporate the changing mesoscale atmospheric environment, as well as focus down to the metre-sized fine dynamic scales of vortices in the fireline through horizontal and vertical grid refinement. It has been used in previous studies (Clark *et al.*, 1996a, and 1996b) to demonstrate the dynamic causes of the bowing of firelines, the formation of vortices within the fireline, and sudden outbursts of small fingers of flame from the fireline. Its contribution to WiFE and other fire experiments will continue to further reveal and explain complex vortex dynamics events such as the FOD.

Extended-Dynamic-Range Imaging Spectrometer (EDRIS)

EDRIS (Riggan *et al.*, 1993), a component of the Airborne Infrared Disaster Assessment System, is a conventional cross-track through nadir scanning imager with a narrow FOV telescope staring at a rotating mirror. Here, we use a visible channel (0.7μm) to reveal location-identifying ground features, together with near IR (1.6μm) and thermal IR (10μm), which bring out smoke and burning regions, respectively. **Figure 8a** is such a composite, which shows portions of the Edna Fire Complex near Banning, California on 6 October 1998. When we arrived, multiple-start fires of mysterious origins had been burning unchecked under Santa Ana winds. In the image, the fire is proceeding down slope, leaving a mostly blackened and charred countryside behind, and moving onto a flatter flood plain that is intensively farmed. Several active fires can be seen at its wedge-shaped head (arrow). A number of less intense fires burn toward the right of the image. Repeated passes reveal this to have been a dangerous period, with the head of the fire advancing at nearly $1 ms^{-1}$. EDRIS spectral capability is also very well illustrated here because the visible channel allows the user to clearly identify buildings and highways, an advantage that is made clear in the passive microwave image discussion that follows.

EDRIS has also played a key role in evaluating the impact of the FOD vortex. Specifically, while the FOD vortex withdraws nearly as rapidly as it moved forward (**Figure 7**, Frame 6), a poorly resolved ghost-like thermal remnant is evident in its wake. This feature hints at the possibility that the vortex had ignited new fires extending well beyond the head of the crown

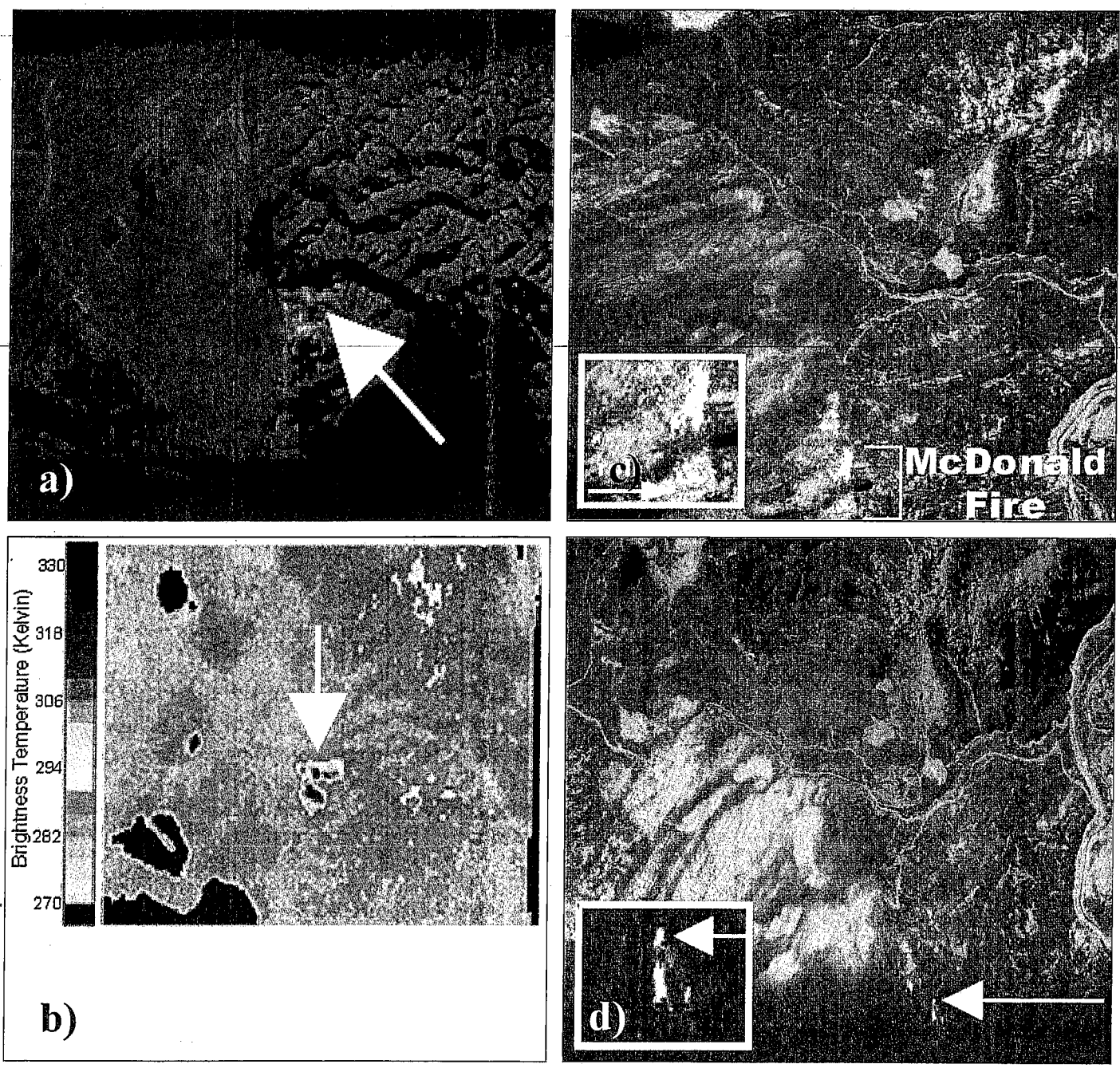

Figure 8.
EDRIS spectral image (a) and AIMR passive microwave image (b) of the Edna Fire complex. Arrows mark the wedge-shaped region off the actively advancing fire. The black features in the lower left of 8b show cooler temperature agricultural ponds. Frames 8c and 8d are EDRIS time sequence images of the McDonald Fire complex. The fire advance following the Finger of Death (FOD) vortex can be clearly seen in the inset square in Figure 8d.

fire along its line of advance. At this experimental juncture, the multi-sensor WiFE payload provides additional and critical support to our observations. The C-130, shortly after imaging the FOD, inadvertently drifted off its pylon turn, necessitating breaking off its nearly fixed pattern orbiting the fires. Returning, we made a sequence of three straight and level passes over the fire complex; these were optimal for the nadir scanning imagers and the NASA/USDA Forest Service EDRIS, which acquired excellent overviews of the McDonald Creek fire and key data in the aftermath of the FOD.

In **Figure 8c**, with pixel size of approximately 5 m, we see the three actively burning areas of the fire complex. The fire at the bottom of the figure marked McDonald is the crown fire in **Figure 6**, but prior to the period of extreme behaviour shown in **Figure 6**. In **Figure 8d** we see the McDonald fire again, note the slight change in perspective, some minutes after our observation of the FOD. The image is a very useful composite of visible (channel 1), near IR (channel 2), and 10μm (channel 3) as red, green, and blue (RGB), respectively. This allows us to see the low-level smoke plume (light blue), the heavily

forested zones (green/black), the river and riverbed (blue/green), and the fire in thermal IR/10μm (red, yellow, and white). The image is 4.6 minutes after the sequence shown in **Figure 7**, Frame 6. One of the dramatic horizontal roll-like features can be just barely seen in the inset of **Figure 8c**.

In **Figure 8d**, eighteen minutes after observing the FOD, the crown fire had substantially decreased in overall intensity, smoke output had decreased strikingly, and the intense horizontal roll features had diminished, but most importantly, along the path of the FOD, a newly-ignited street of fire lay ahead of the original fireline. The inset in **Figure 8d** enlarges this singular feature. The new fireline is marked with an arrow in both the inset and at full scale in **Figure 8d**.

The data combined from these two remote sensors, TCAM and EDRIS, with their very different temporal scales, resolved an important issue: the FOD vortex at the head of the wildfire had indeed advanced the head of the fire, very probably, by 100 m or more in a single stroke.

There are several aspects of our observations of extreme fire behaviour at the McDonald Creek fire that deserve additional attention. The remarkable and dangerous flame filled FOD and its ability with a single 150 m bound to defeat any reasonable firebreak is an important new observation of extreme fire behaviour. However, the FOD did not occur without two instructive warnings. The first of these cautionary warnings was the Forest Services forecast characterization of hazard potential rating designating this a "red flag day". This is their highest alert of potential extreme fire behaviour, a warning that these observations amply verify. A second warning is found in our IR images of the horizontally oriented wave-like sequence perpendicular to the direction of the advancing wildfire. The roll features and their apparent falling vortex caps provide ample indication of the rapid production of vorticity that could culminate in the extreme FOD. From this aspect alone, the use of airborne IR remote sensors at high temporal and spatial resolution aboard fire suppression tactical guidance aircraft could be justified.

Airborne Imaging Microwave Radiometer (AIMR)

For normal terrestrial temperatures of ~280°K, the thermal IR band peaks at 10μm. Fortunately, the Plank distribution slopes more shallowly toward the microwave region, making passive microwave imagers of modest size practical. Coupling the atmosphere's transparency together with modern microwave receiver technology, AIMR scans ± 60° cross-track and is corrected by inertial reference for both roll and yaw. Its 3 dB beam width of 1° at 90 GHz gives a 50 m footprint at our typical operating altitude of 3 km A.G.L.. AIMR's 37 and 90 GHz frequencies are nearly optimal for terrestrial observations. However, when compared to thermal IR technology, modern microwave digitally controlled receivers offer a very substantial advantage in dynamic range for studying wildfires. NCAR's AIMR[1] covers from -20°C to 1500°C. **Figure 8b** shows the same scene as in **Figure 8a** at a slightly different scale. This frame is the average of both polarizations at 97 GHz. The agricultural ponds in the lower left can be immediately recognized (cool features).

Orientation within an AIMR image is generally more difficult than in the spectral EDRIS image (**Figure 8a**). In this EDRIS image, the thermal channel showing the fire's hot spots are overlaid in green and yellow. Note the scattered fires (green area to the left of centre) remaining active in the Edna's fire's wake. The fire is burning from right to left across the figure. This orientation problem is largely an image interpretation problem. In the EDRIS composite image the scene appears much as seen by unaided vision, but with the obscuring smoke largely removed, the firelines highlighted, and geographical features easily identified. The passive microwave images, as displayed (**Figure 8b**), while rich in textured features are not so immediately assimilated and recognized. However, the wedge-shaped actively burning areas marked with arrows in **Figures 8a** and **8b** are clearly depicted, as are the many hot spots left smouldering following the fire's passage. Both of these images illustrate the challenge that a wildfire presents to suppression efforts when driven by a strong wind. New fires have been spotted all across this ~8x8 km frame. Several of these fires spawned rapid advances while we observed, but none were observed to extend into the agricultural region, stopped here by natural and manmade barriers.

Passive Microwave Observations of Biomass Distribution

One of the critical challenges in modelling wildfire behaviour is to determine the surface distributions and amounts of biomass fuel in the fire's path. As the amounts of biomass are important to agricultural, forestry and climate change interests, there has been considerable research on remote sensing techniques for use in mapping biomass amounts. Amongst the most promising techniques are microwave active and passive technologies (Imhoff, 1995). For heavy stands of timber, radar offers a direct measure of the backscatter coefficient that when choosing appropriate wavelengths, should depend closely on the amounts and sizes of the biomass backscattering elements. Obviously, longer wavelengths, being more sensitive to the larger structures (*e.g.* tree trunks), several wavelengths and knowledge of the distribution of backscatter elements within the forest or target will be required for an unambiguous estimate of biomass amount (Larsson *et al.*, 1999). However, various high-resolution multi-spectral vegetation classification schemes coupled with prior knowledge of the biomass fuel species present in the location of interest, may represent a more immediately practical approach (Gougeon, 1995 and Leckie *et al.*, 1995).

[1]The AIMR was originally built by MPB Technologies as AIMR and has recently been modernized and rebuilt by NCAR's Remote Sensing Facility and is on loan to NCAR from the Meteorological Services, Canada.

These observational demands of using radar for biomass estimation are sufficiently severe that we have examined the potential of using passive microwave techniques and existing hardware held at NCAR. Choudhury (1990) and Smith and Choudhury (1990 and 1993) have suggested that in viewing the earth surface at 37 GHz (8mm wavelength) the difference in radiometric brightness temperatures at vertical and horizontal polarizations would be a measure of surface characteristics (emissivity), vegetation geometry and woody biomass. The polarization difference (PD) should be high for flat featureless surfaces such as sandy desert, snow or calm water (25°-35° K) based on physical principles. The highest values of PD found by the Nimbus 7 Scanning Multi-channel Microwave Radiometer (SMMR) globally were measured above bodies of water. PD decreases monotonically with increasing biomass and structural complexity. Bio-structures at the scale of the wavelength 8 mm/37 GHz such as stems and foliage will have a modestly disproportionate contributions, as would grasses. At 3 mm/90 GHz, branches and brush will be more important. Global maps of PD (at 37 GHz) from the Nimbus 7 SMMR (Choudhury, 1993) closely resemble maps of vegetation amounts from other sources and clearly identify with a S/N of better than one part in twenty, the differences between zero vegetation, grasslands, temperate forest and tropical rain forests. The extremely dense and complex canopy structures of the tropical rain forests yield a PD of only a few degrees. From the standpoint of wildfire behaviour and modelling, this level of biomass amount discrimination seems entirely adequate. Hence, we will evaluate the potential of the NCAR passive microwave radiometer (AIMR) that the WiFE team is also using for fire mapping as a biomass mapper.

As **Figure 9** was recorded, the C-130 was flying over the eastern flanks of the Bernadiume Mountains east of Banning, CA as the terrain descends onto an agricultural alluvial plain. The AIMR's spatial resolution is about 50m and PD is accurate to ~1°K. The largest values of PD (zero biomass) are observed from the three large agricultural ponds along the left flank of the image (**Figures 8a** and **8b**). The ponds appear here as black features. In the upper right quadrant of **Figure 9** are two regions marked as "fire scars". They roughly follow the blackened zones in **Figure 8a** that lead to the still advancing head of the Edna fire. These fire scars have been denuded by the fire within hours and now have a substantially higher PD value than their surroundings (some standing charred materials remain). In contrast, the lower right quadrant with its scrub in medium terrain ecology, is mostly untouched by the fire and only burned in scattered locations, but shows a lower PD, hence a higher biomass content. The noisy vertical track slightly left of centre in **Figure 9** is data from very near nadir and must be disregarded as a technical artifact.

Our use of PD as a fuel estimate remains a work in progress and data from two "calibrated" experimental forest plots provide promise of a usable calibration factor, but for the moment PD from the AIMR offers considerable promise as a land use and fire research tool.

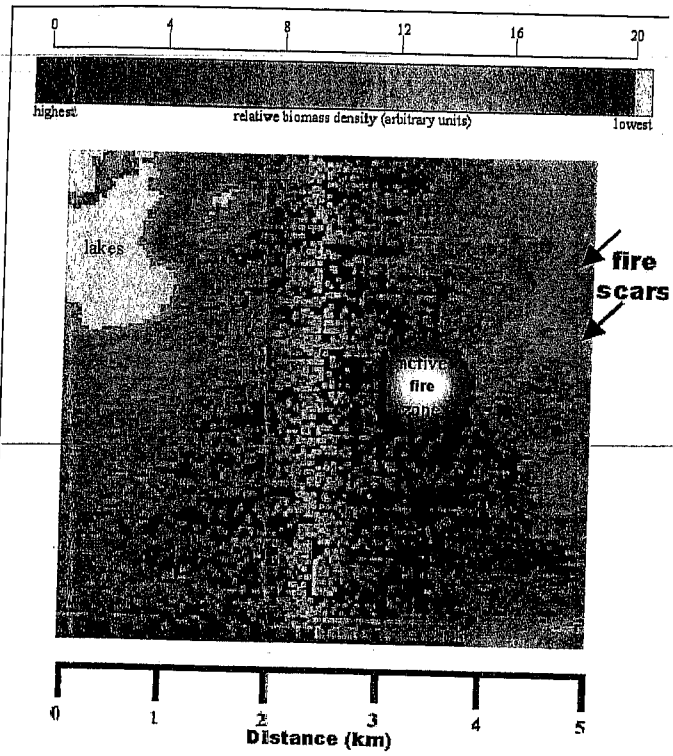

Figure 9.
Microwave Polarization Difference, in degrees Kelvin. The recent fire scars show significantly reduced biomass density.

CONCLUSIONS

The Wildfire Experiment was designed as both a research program and as a feasibility and technology demonstration of real-time airborne remote sensing in fire research. Each of the sensors produced usable quantitative fire data as false colour imagery in real-time aboard the aircraft, but the optical and microwave line scanners produced only a single image with each straight and level pass over the fire. The NASA/USDA Forest Service developed EDRIS, a spectral scanner which overlaid visible and IR images into an immediately intelligible composite, lacked only a GIS map overlay to create the perfect situational display from either a fire-fighter's or researcher's perspective.

The microwave imager AIMR, with only a 1° antenna beam width, but extraordinary temperature dynamic range, was unfortunately only operational on relatively low intensity fires with narrow linear features and has yet to fully prove its value as a fire research tool. However, with digital roll and pitch corrections, and polarization diversity, it offers a potential means to map fuel mass distributions using the difference in horizontal and vertical polarization brightness temperatures (PD). This algorithm is currently under development using observations of quantitatively surveyed forest plots in both Montana and California. In some contrast to the large image pixels (approximately one metre) of AIMR and EDRIS, the high-speed digital IR images of the video camera-sized TCAM have obvious applications in airborne platforms much smaller than C-130s. However, it was the TCAM's small size and

mechanical pointability that allowed us in the pylon-turning C-130 to continuously image large fires at 30 Hz and up to 60 Hz for periods approaching 30 minutes. Importantly, the most vigorous and dynamic fires observed were almost completely shrouded by smoke. Indeed, a co-aligned colour video camera could see nothing of the dangerous and dynamic fire behaviour documented, perhaps for the first time, by the TCAM.

Numerical techniques, which largely removed aircraft motions from the earth reference TCAM images, together with image flow analysis have allowed a remarkable new perspective of air motions in and around wildfires, and have clearly revealed several exciting vortex phenomena relevant to both fire spread and safety near large fires. In combination, this suite of remote sensors has together confirmed a role in rapid-fire spread by the explosively extending, fire-filled, horizontal vortices and related phenomena.

We envision that as coupled atmospheric-fire behaviour models become more realistic, an airborne remote sensing payload such as used here during WiFE will have a key role in fire model verification.

ACKNOWLEDGEMENTS

Thanks are due to Mr. Matt McGinity of Inframetrics, Inc. for his advice and many kindnesses, to the anonymous reviewers for their care and attention, and to Terri Cantrell for her patience and skill in revisions. Thanks are also due to the Research Aviation Facility and the Remote Sensing Facility of the National Center for Atmospheric Research. Special thanks to the pilots and crew of the National Science Foundation's C-130Q who endured seemingly endless smokey pylon turns. Thanks also to Vince Ambrosia at NASA Ames Research Center for reanalysis of EDRIS data.

REFERENCES

Bab-Hadiashar, A., and D. Suter. (1995). "2-D Motion Extraction Using an Image Interpolation Technique". *The International Society for Optical Engineering (SPIE): Applications of Digital Image Processing XVIII*, ed. A. G. Tescher, SPIE, pp. 271-281.

Bab-Hadiashar, A., and D. Suter. (1997). "Optic Flow Calculation Using Robust Statistics", *Computer Vision & Pattern Recognition (CVPR) Conf.*, The Institution of Electrical and Electronics Engineers Computer Society, Puerto Rico, June, pp. 988-993.

Choudhury, B.J. (1990). Part VI: Land: "Desertification", *Atlas of Satellite Observations Related to Global Change*, eds. R. J. Gurney, J. L. Foster, and C. L. Parkinson, Cambridge Press, NY, pp. 470.

Choudhury, B.J.. (1993). "Reflectivities of Selected Land Surface Types at 19 and 37 GHz from SSM/I Observations", *Remote Sensing of the Environment.*, Vol. 46, No. 1, pp. 1-17.

Clark, T.L., M.A. Jenkins, J. Coen, and D. Packham. (1996a). "A Coupled Atmospheric-Fire Model: Convective Feedback on Fireline Dynamics", *Journal of Applied Meteorology*, Vol. 35, pp. 875-901.

Clark, T.L., M.A. Jenkins, J. Coen, and D. Packham. (1996b). "A Coupled Atmospheric-Fire Model: Role of the Convective Froude Number and Dynamic Fingering at the Fireline", *International Journal of Wildland Fire*, Vol. 6, pp. 177-190.

Clark T.L., J.L. Coen, L. Radke, M. Reeder, and D. Packham. (1998). "Coupled Atmosphere-Fire Dynamics", *3rd Int. Conf. on Forest Fire Research*, American Meteorological Society (Boston, MA), Coimbra, Portugal, pp. 67-82.

Clark T., L. Radke, J. Coen, and D. Middleton. (1999). "Analysis of Small-Scale Convective Dynamics in a Crown Fire Using Infrared Video Camera Imagery", *Journal of Applied Meteorology*, Vol. 38, pp. 1401-1420.

Gougeon, F.A. (1995). "Comparison of Possible Multispectral Classification Schemes for Tree Crowns Individually Delineated on High Spatial Resolution MEIS Images", *Canadian Journal of Remote Sensing*, Vol. 21, No. 1, pp. 1-9.

Haines, D.A. (1987). "Three Types of Horizontal Vortices Observed in Wildland Mass and Crown Fires", *Journal of Climate and Applied Meteorology*, Vol. 26, No. 12, pp. 1624-1637.

Horn, B.K.P., and B.G. Schunck. (1981). "Determining Optical Flow", *Artificial Intelligence*, Vol. 17, pp. 185-204.

Imhoff, M. (1995). "Radar Backscatter and Biomass Saturation: Ramifications for Global Biomass Inventory", *IEEE Trans. on Geoscience and Remote Sensing*, Vol. 33, pp. 511-518.

Larsson, B., B. Flood, P-O Frölind, A. Gustavsson, H. Hellsten, M. Herbertsson, T. Jonsson, O. Seger, G. Smith, G. Stenström, and L.M.H. Ulander. (1999). "VHF SAR for Foliage Penetration (FOPEN) and Forest Biomass Estimation", *Proc. 4th International Airborne Remote Sensing Conference and Exhibition / 21st Canadian Symposium on Remote Sensing*, Ottawa, Ontario, Canada (ERIM, Ann Arbor, MI), Vol. 1, pp. I 853-I 860.

Leckie, D.G., J. Beaubien, J.R. Gibson, N.T. O'Neill, T. Piekutowski, and S.P. Joyce. (1995). "Data Processing and Analysis for MIFUCAM: A Trial of MEIS Imagery for Forest Inventory Mapping", *Canadian Journal of Remote Sensing*, Vol. 21, No. 3, pp. 337-356.

Nagel, H.-H. (1983). "Displacement Vectors Derived from Second-Order Intensity Variations in Image Sequences", *Computer Vision Graphics & Image Processing*, Vol. 21, pp. 85-117.

National Interagency Fire Coordination Center, cited. (1998). "The McDonald Creek Fire in the Kootenai Complex", [Available on-line from http://www.nifc.gov/sitreport].

Pyne, S.J., P.L. Andrews and R.D. Laven. (1996). "Introduction to Wildland Fire", 2nd edition, John Wiley and Sons, Inc. New York, 769 p.

Radke, L., D. Hegg, J. Nance, P. Hobbs, K. Laursen, R. Weiss, P. Riggan, and D. Ward. (1991). Chapter 28: "Particulate and Trace Gas Emissions from Large Biomass Fires in North America", *Global Biomass Burning: Atmospheric, Climatic, and Biospheric Implications*, ed. J. S. Levine, MIT Press, Cambridge, MA, pp. 569.

Riggan, P.J., J.A. Brass, and R.N. Lockwood. (1993). "Assessing Fire Emissions from Tropical Savanna and Forests of Central Brazil", *Photogrammetric Engineering & Remote Sensing*, Vol. 59, No. 6, pp. 1009-1015.

Scorer, R.S. (1978). *Environmental Aerodynamics*, Ellis Horwood Ltd. (Halsted Press book), Chichester, Eng., pp. 487.

Smith, E.A., and B.J. Choudhury. (1993). "The Relationship Between Anomalies of Interannual Net Radiation and 37 GHz Polarization Difference Over North Africa", *Climate Change*, Vol. 23, No. 2, pp. 141-154.

Smith, R.C.G., and B.J. Choudhury. (1990). "Relationship of Multispectral Satellite Data to Land Surface Evaporation from the Australian Continent", *International Journal of Remote Sensing*, Vol. 11, No. 11, pp. 2069-2088.

Verri, A., F. Girosi, and V. Torre. (1990). "Differential Techniques for Optical Flow", *Journal of the Optical Society of America*, Vol. 7, pp. 912-922.